Simultaneous nonreciprocal conventional photon blockades of two independent optical modes by a two-level system

Yu-Mu Liu,[1] Jing Cheng,[1] Hong-Fu Wang,[1,2,*] and Xuexi Yi[1,†]

[1]*Center for Quantum Sciences and School of Physics, Northeast Normal University, Changchun 130024, China*

[2]*Department of Physics, College of Science, Yanbian University, Yanji, Jilin 133002, China*

(Received 11 January 2023; accepted 23 May 2023; published 2 June 2023)

We propose a scheme to achieve nonreciprocal conventional photon blockades simultaneously in two independent optical modes, which are connected by a two-level system. In the case that only one optical mode is weakly driven, we find that strong nonreciprocal photon blockades of both optical modes can be observed. We show that, for both optical modes, the single-photon blockades happens by driving the nonlinear device from one side, while photon-induced tunneling appears when driving the system from the other side, which is attributed to the anharmonic eigenenergy spectrum constructed by resonantly coupling to a two-level system. According to photon resonance transition processes under different driving directions, the four optimal Fizeau-Sagnac shifts can be obtained to generate perfect nonreciprocal conventional photon blockades of both optical modes. Our study opens an avenue to simultaneously manipulate multiple nonreciprocal single-photon devices and may have potential applications in chiral quantum information processing.

DOI: 10.1103/PhysRevA.107.063701

I. INTRODUCTION

In recent years, significant progress has been made in creating and manipulating single-photon sources utilizing optical nonlinearity for their importance in quantum information processing, which has a profound impact on future optical devices [1,2]. Realizing high-purity single-photon sources is essential in the field of modern optical technologies such as single-photon transistors [3,4], quantum repeaters [5], quantum optical Josephson interferometers [6], and nonclassical optical isolators and circulators [7].

Researchers recently found that the single-photon source can be generated by optical nonlinearity, such as the photon blockade effect [8–11], which opens up a completely new route toward nonlinear quantum optics. It is a purely quantum phenomenon, where the absorption of the first photon will block the transmission of subsequent photons. This effect can be used for realizing quantum information processing, including the development of single-photon transistors [12], which is one of the long-term goals of quantum optics. So far, many schemes based on the photon blockade effect have been studied by utilizing different physical devices, including cavity quantum electrodynamics (QED) systems [10,13,14], coupled cavities [15], the Rydberg atom [16,17], optomechanical system [18,19], and so on. Among them, according to the underlying physical mechanism, photon blockade can be roughly divided into two types: conventional photon blockade [20–22] and unconventional photon blockade [23–26]. The first depends on the anharmonicity between the energy levels of the system, while the second relies on the destructive quantum interference between distinct driven-dissipative pathways. By far, the conventional photon blockade is studied in an optical cavity coupled to a single trapped atom [8], circuit quantum electrodynamical systems [13,27], and photonic crystal systems [28]. In addition, a more significant energy-level splitting induced by the nonlinearity of the system can be constructed via the dispersive coupling between the optical field and the qubit to realize the conventional photon blockade effect [29,30]. On the other hand, by constructing multiple interference paths via the auxiliary cavity [25,31,32], unconventional photon blockade has also been widely reported in which weak nonlinearity is required. According to the authors of Ref. [33], although strong optical nonlinearity of the system is not required in the unconventional photon blockade effect, it exhibits higher-order bunched photons, which may not be an excellent way to generate single-photon sources [34].

Optical reciprocity is required for the function and analysis of physical systems [35,36], but with the rise of nonreciprocal devices [37–39], breaking it can also be beneficial in quantum optics. For example, nonreciprocal devices play an essential role in signal processing and invisible sensing [40] and can protect laser sources from noise, which are core components in an integrated photonic circuit [41,42]. Thus, as one of the effective means of generating nonreciprocal single-photon sources [43], the nonreciprocal photon blockade effect [44] has been studied by using rotating resonators. So far, most studies on nonreciprocal photon blockade were focused on photon nonreciprocal statistical properties in a single optical mode [44–47], however, simultaneous nonreciprocal photon blockades of both independent optical modes have not been reported.

In this paper, we study the possibility of achieving simultaneous nonreciprocal photon blockades of both independent

*hfwang@ybu.edu.cn

†yixx@nenu.edu.cn

optical modes via a rotating optical device and a two-level system. The two-level system acts as the nonlinear medium that mediates the transformation of the photons between the two uncoupled optical modes. The four optimal solutions for Fizeau-Sagnac shifts can be analytically obtained based on single-photon and two-photon resonance transition processes under different driving directions. By calculating the equal-time second-order correlation function analytically and numerically, we find that simultaneous single-photon blockade and photon-induced tunneling for both optical modes can occur in the spinning resonator, that is, simultaneous nonreciprocal photon blockades can be found. According to the energy spectrum of the system, the physical origins behind the observed phenomena are well discussed. Compared with the previous photon blockade schemes, our scheme has the following distinct advantages.

(i) There is no need to drive the two-level system but the strong photon blockade and nonreciprocal photon blockades can still be observed in the both optical modes.

(ii) Even though the two optical modes are uncoupled from each other directly, excellent nonreciprocal conventional photon blockades can be observed simultaneously in both optical modes.

Here we should point out that, compared with the previous nonreciprocal photon blockade schemes [34,44–48], the present scheme has the distinct advantage of achieving nonreciprocal photon blockade in multiple independent optical modes simultaneously, which has practical research significance in many-body quantum information processing, complex quantum communication, and quantum computing.

The paper is organized as follows. In Sec. II, we introduce the physical model and present the Hamiltonian in a rotating optical cavity and a two-level system. In Sec. III, we derive the four optimal Fizeau shifts for the nonreciprocal conventional photon blockade and analytically solve the equal-time second-order correlation function of both independent optical modes in detail. In Sec. IV, by calculating the equal-time second-order correlation function, we discuss the simultaneous nonreciprocal conventional photon blockades effect of both independent optical modes and explain the physical origin behind the observed phenomena. Finally, we give a brief conclusion in Sec. V.

II. PHYSICAL MODEL

Figure 1 shows our setup, a two-level system with an excited state $|e\rangle$ and a ground state $|g\rangle$ is coupled to the two independent optical modes a_1 and a_2 simultaneously. An external classical light with frequency ω_l and amplitude E can be coupled into and out of the rotating cavity by using an optical fiber. The total Hamiltonian of the entire hybrid system is ($\hbar = 1$)

$$H_{\rm tot} = H_{\rm sys} + H_{\rm probe}, \tag{1}$$

with

$$\begin{aligned} H_{\rm sys} &= (\omega_{c1} + \Delta_{\rm F1})a_1^\dagger a_1 + (\omega_{c2} + \Delta_{\rm F2})a_2^\dagger a_2 \\ &\quad + \omega_0\sigma_+\sigma_- + J(a_1\sigma_+ + a_2\sigma_+ + {\rm H.c.}), \\ H_{\rm probe} &= E(a_1^\dagger e^{-i\omega_l t} + a_1 e^{i\omega_l t}), \end{aligned} \tag{2}$$

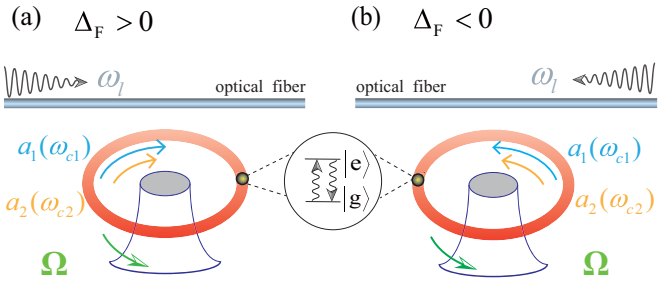

FIG. 1. Schematic diagram of a two-level system with a ground state $|g\rangle$ and an excited state $|e\rangle$ coupled to a rotating optical cavity. There are two independent optical modes a_1 with frequency ω_{c1} and a_2 with frequency ω_{c2} in the rotating optical cavity, which are rotating in the same direction. The external driving field with frequency ω_l is coupled in and out of the optical mode a_1 with frequency ω_{c1} through a tapered optical fiber. The rotating optical cavity spins at a certain angular velocity Ω. (a) The device is driven from the left side ($\Delta_{\rm F} > 0$). (b) In the case of driving the device from the right side ($\Delta_{\rm F} < 0$).

where a_j ($a_j^\dagger$) represents the annihilation (creation) operator of the jth optical mode with frequency ω_{cj} ($j = 1, 2$). $\sigma_+ = |e\rangle\langle g|$ ($\sigma_- = |g\rangle\langle e|$) refers to the raising (lowering) operators of the two-level system with resonant transition frequency ω_0. The parameter J signifies the coupling strength between the two-level system and optical modes, which results in an anharmonic energy-level structure. $E = \sqrt{2P\kappa_1/\hbar\omega_l}$ is the coupling between the optical mode a_1 with dissipation rate κ_1 and the external driving laser with frequency ω_l and power P. As a result of the cavity rotating at a fixed angular velocity Ω, both optical modes experience a Fizeau shift $\Delta_{\rm Fj}$, which leads to $\omega_{cj} \to \omega_{cj} + \Delta_{\rm Fj}$. According to the authors of Ref. [44], the concrete expression form of $\Delta_{\rm Fj}$ is determined by

$$\Delta_{\rm Fj} = \pm\frac{nr\Omega\omega_{cj}}{c}\left(1 - \frac{1}{n^2} - \frac{\lambda}{n}\frac{dn}{d\lambda}\right), \tag{3}$$

where n represents the refractive index experienced by clockwise or counterclockwise optical modes and r is the radius of the cavity. c and λ are the speed and wavelength of light in a vacuum, respectively. The Lorentz corrections are applied to Fresnel-Fizeau drag coefficients by the dispersion term $(\lambda/n)(dn/d\lambda)$, which is usually negligible in typical materials [49]. The rotation direction of the resonator can be fixed counterclockwise for convenience, the sign of Fizeau shift $\Delta_{\rm Fj}$ is determined by the direction of light propagation, that is, the propagation direction of light along ($\Delta_{\rm Fj} < 0$) or against ($\Delta_{\rm Fj} > 0$) the rotation direction of the spinning resonator. For simplicity, we set the frequencies of both optical modes to be identical later ($\omega_{c1} = \omega_{c2} = \omega_c$), i.e., $\Delta_{\rm F1} = \Delta_{\rm F2} = \Delta_{\rm F}$.

In a frame rotating at driving frequency ω_l, the total Hamiltonian of the system becomes time independent

$$\begin{aligned} H'_{\rm tot} &= (\Delta_c + \Delta_{\rm F})a_1^\dagger a_1 + (\Delta_c + \Delta_{\rm F})a_2^\dagger a_2 + \Delta_0\sigma_+\sigma_- \\ &\quad + J(a_1\sigma_+ + a_2\sigma_+ + {\rm H.c.}) + E(a_1^\dagger + a_1), \end{aligned} \tag{4}$$

$\Delta_c = \omega_c - \omega_l$ ($\Delta_0 = \omega_0 - \omega_l$) is the corresponding cavity (two-level system)-driven laser detuning. Next, we examine the statistical properties of both independent optical modes and explore their nonreciprocal properties separately.

III. PHOTON STATISTIC

In this section, we obtain the optimal Fizeau shifts for simultaneous nonreciprocal photon blockades of the both optical modes by analyzing the eigenenergy spectrum of the system in detail. The second-order correlation function for quantifying the statistical properties of the photons can be analytically obtained by solving the non-Hermitian Schrödinger equation.

A. Optimal Fizeau-Sagnac shifts

To obtain the optimal Fizeau shifts for nonreciprocal conventional photon blockades, the eigenequation of the system is introduced as follows [50]:

$$H_k|\psi_k\rangle = E_k|\psi_k\rangle, \tag{5}$$

where $|\psi_k\rangle$ represents the eigenstate of the system and E_k denotes the eigenenergies ($k = 0, 1, 2,...,$). The Fock-state basis of the multimodes system can be described by $|mng\rangle$ ($|mne\rangle$), with the number m (n) denoting the photon number in the optical mode a_1 (a_2) and g (e) denoting the two-level system in the ground (excited) state. It can be clearly seen that the excitation number operator $N = a_1^\dagger a_1 + a_2^\dagger a_2 + \sigma_+\sigma_-$ is a conserved quantity because of the commutative relation $[H_{\rm sys}, N] = 0$ [21]. The subspaces corresponding to different weighted excitation number N are separated from each other so that one can obtain the k-photon resonance conditions in different subspaces [51]. In the weak driving limit, the Hamiltonian can be expanded with one-excitation subspace bases $\{|10g\rangle, |01g\rangle, |00e\rangle\}$ in the following matrix form:

$$H_1 = \begin{bmatrix} \omega_c + \Delta_{\rm F} & 0 & J \\ 0 & \omega_c + \Delta_{\rm F} & J \\ J & J & \omega_0 \end{bmatrix}. \tag{6}$$

Here the subscript 1 indicates the one-photon excitation subspace. For simplicity, we assume $\omega_c = \omega_0$ in the following discussion, i.e., $\Delta_c = \Delta_0 = \Delta$. The eigenvalues E_1 of the Hamiltonian H_1 can be obtained by $|H_1 - E_1 I| = 0$, where I is the identity matrix. When the driving field frequency ω_l is equal to the eigenvalue E_1 ($\omega_l = E_1$), the single-photon resonance condition is satisfied. Thus, the cavity detunings $\Delta_1^{(k)}$ with respect to the driving frequency ω_l in one-photon transition processes can be obtained as follows:

$$\begin{aligned} \Delta_1^{(1)} &= -\Delta_{\rm F}, \\ \Delta_1^{(2,3)} &= \frac{-\Delta_{\rm F} \mp \sqrt{8J^2 + \Delta_{\rm F}^2}}{2}, \end{aligned} \tag{7}$$

and the corresponding normalization eigenstates are

$$\begin{aligned} |\psi_1^{(1)}\rangle &= \frac{1}{\sqrt{2}}(-|10g\rangle + |01g\rangle), \\ |\psi_1^{(2)}\rangle &= \frac{1}{\sqrt{B_1}}\left(\frac{-2J}{B_2}|10g\rangle - \frac{2J}{B_2}|01g\rangle + |00e\rangle\right), \\ |\psi_1^{(3)}\rangle &= \frac{1}{\sqrt{B_3}}\left(\frac{B_2}{2}|10g\rangle + \frac{B_2}{2}|01g\rangle + 2J|00e\rangle\right), \end{aligned} \tag{8}$$

with

$$\begin{aligned} B_1 &= 1 + \frac{8J^2}{B_2^2}, \\ B_2 &= \Delta_{\rm F} + \sqrt{\Delta_{\rm F}^2 + 8J^2}, \\ B_3 &= 8J^2 + \Delta_{\rm F} B_2, \end{aligned} \tag{9}$$

where the subscript 1 of the cavity detunings $\Delta_1^{(k)}$ denotes single-photon resonance excitation for both optical modes, which is one of the conditions for achieving conventional photon blockade. In other words, once a specific single-photon resonance condition is satisfied, the photons have an excellent probability of occupying the corresponding eigenstates $|\psi_1^{(k)}\rangle$, which can give rise to the conventional photon blockade phenomenon. However, the photon blockade phenomenon disappears when $\Delta_1 = -\Delta_{\rm F}$, which will be analyzed after solving the two-photon resonance excitation conditions.

Similarly, in the two-excitation subspace with bases $\{|20g\rangle, |02g\rangle, |11g\rangle, |10e\rangle, |01e\rangle\}$, the Hamiltonian can be written in the following matrix form:

$$H_2 = \begin{bmatrix} D_1 & 0 & 0 & \sqrt{2}J & 0 \\ 0 & D_1 & 0 & 0 & \sqrt{2}J \\ 0 & 0 & D_1 & J & J \\ \sqrt{2}J & 0 & J & D_2 & 0 \\ 0 & \sqrt{2}J & J & 0 & D_2 \end{bmatrix}, \tag{10}$$

with

$$\begin{aligned} D_1 &= 2(\omega_c + \Delta_{\rm F}), \\ D_2 &= 2\omega_c + \Delta_{\rm F}. \end{aligned} \tag{11}$$

Here the subscript 2 indicates the two-photon excitation subspace. The eigenvalues E_2 of the Hamiltonian H_2 can be obtained by $|H_2 - E_2 I| = 0$. When the frequency of the drive field ω_l equals one-half of the eigenvalues E_2 ($2\omega_l = E_2$), the two photon resonance condition is satisfied. Thus, the cavity detunings $\Delta_2^{(k)}$ with respect to the driving frequency ω_l in two-photon transition processes can be obtained as follows:

$$\begin{aligned} \Delta_2^{(1)} &= -\Delta_{\rm F}, \\ \Delta_2^{(2,3)} &= \frac{-3\Delta_{\rm F} \mp \sqrt{8J^2 + \Delta_{\rm F}^2}}{4}, \\ \Delta_2^{(4,5)} &= \frac{-3\Delta_{\rm F} \mp \sqrt{16J^2 + \Delta_{\rm F}^2}}{4}, \end{aligned} \tag{12}$$

where the subscript 2 of the cavity detunings $\Delta_2^{(k)}$ denotes two-photon excitation. Equation (12) also represents the processes of the two-photon resonance excitation, that is, the photons have a great probability of being located in the two-photon state, which leads to the emergence of photon-induced tunneling. Notably, by comparing Eqs. (7) and (12), we find that $\Delta_1^{(1)} = \Delta_2^{(1)}$, which implies the disappearance of the effect of the single-photon blockade because of the two-photon resonance transition.

It can be easily found that $\Delta_1^{(2,3)} \neq \Delta_2^{(2,3)} \neq \Delta_2^{(4,5)}$ in the real space by Eqs. (7) and (12), which means that the one-

and two-photon resonance conditions cannot be satisfied simultaneously, that is, the optimal nonreciprocal conventional photon blockade cannot be achieved. In other words, the optimal nonreciprocal conventional photon blockade requires $\Delta_1^{(2,3)} = \Delta_2^{(4,5)}$ when driving devices from different directions. More importantly, in the present scheme, the sign of the Δ_F can be changed due to the different directions of the propagation of the light, which makes $\Delta_1^{(2,3)} = \Delta_2^{(4,5)}$ possible in the real space. Concretely, assuming that a certain one-photon resonance process is satisfied when the device is driven from the left-hand side ($\Delta_F > 0$), for example, $\Delta_L = \Delta_1^{(2)} = \frac{-\Delta_F - \sqrt{8J^2+\Delta_F^2}}{2}$, where the subscript L represents the system driven from the left-hand side. One can set $\Delta_F = y \times J$ ($y \in \mathcal{R}$), so that $\Delta_L = \Delta_1^{(2)} = \frac{-(y\times J) - \sqrt{8J^2+(y\times J)^2}}{2}$. At the same time, it is assumed that a certain two-photon resonance process is satisfied when the device is driven from the right-hand side ($\Delta_F < 0$), for example, $\Delta_R = \Delta_2^{(4)} = \frac{-3\Delta_F - \sqrt{16J^2+\Delta_F^2}}{4}$, where the subscript R represents the driving system from the right-hand side. In this case, one can set $\Delta_F = -y \times J$ ($y \in \mathcal{R}$), so that $\Delta_R = \Delta_2^{(4)} = \frac{-3(-y\times J) - \sqrt{16J^2+(-y\times J)^2}}{4}$. It should be emphasized that the difference in the sign of Δ_F results from the difference in the driving direction.

To observe the nonreciprocal photon blockade under the same optical detuning, one can set $\Delta_L = \Delta_R$. Then we can obtain optimal Sagnac-Fizeau shifts by solving the equation about y,

$$\Delta_{\mathrm{Fopt}}^{(1)} = \pm\sqrt{3 - \frac{5}{\sqrt{3}}} \times J,$$
$$\Delta_{\mathrm{Fopt}}^{(2)} = \pm\sqrt{3 + \frac{5}{\sqrt{3}}} \times J. \tag{13}$$

Two such groups of different optimal Fizeau-Sagnac shifts Δ_{Fopt} induce simultaneous nonreciprocal conventional photon blockade of both independent optical modes when driving the device from different directions.

B. Analytical results

To quantitatively study the quantum statistics of the photons, the state vector method is used to analyze the quantum statistics of photons [52]. According to the quantum-trajectory method [53], the non-Hermitian Hamiltonian containing system dissipations can be written as follows:

$$H_{\mathrm{NM}} = H'_{\mathrm{tot}} - i\frac{\kappa_1}{2}a_1^\dagger a_1 - i\frac{\kappa_2}{2}a_2^\dagger a_2 - -i\frac{\gamma}{2}\sigma_+\sigma_-, \tag{14}$$

where κ_1 (κ_2, γ) is the dissipation rate of mode a_1 (a_2, σ). In the weak driving limit, the weak driving term can be considered as a perturbation, thus the wave function of the system at any time can be approximately expressed as [54]

$$\begin{aligned}|\psi(t)\rangle = {} & C_{00g}(t)|00g\rangle + C_{10g}(t)|10g\rangle + C_{01g}(t)|01g\rangle \\ & + C_{00e}(t)|00e\rangle + C_{20g}(t)|20g\rangle + C_{02g}(t)|02g\rangle \\ & + C_{11g}(t)|11g\rangle + C_{10e}(t)|10e\rangle + C_{01e}(t)|01e\rangle,\end{aligned} \tag{15}$$

with probability amplitude $C_{mng(e)}(t)$, which satisfies $\{C_{20g}(0), C_{02g}(0), C_{11g}(0), C_{10e}(0), C_{01e}(0)\} \ll \{C_{10g}(0), C_{01g}(0), C_{00e}(0)\} \ll C_{00g}(0) \approx 1$, that is, the probability of the system is initially in a one-excitation subspace much larger than the two-excitation subspace when $E/\kappa_j \ll 1$. According to Eqs. (14), (15), and the Schrödinger equation $id|\psi(t)\rangle/dt = H_{\mathrm{NM}}|\psi(t)\rangle$, the evolution equations for the wave-function amplitudes can be obtained. Without the loss of physics, one can set $\kappa_1 = \kappa_2 = \gamma = \kappa$. Thus, the analytical results of the probability amplitude can be obtained by using the steady-state assumption as follows:

$$\begin{aligned}C_{10g} &= \frac{2EA_1}{[2(\Delta+\Delta_F)-i\kappa]A_2}, \\ C_{01g} &= \frac{8J^2E}{[2(\Delta+\Delta_F)-i\kappa]A_2}, \\ C_{20g} &= \frac{-2\sqrt{2}E^2((2\Delta-i\kappa)A_3+A_4)}{(2\Delta+2\Delta_F-i\kappa)[A_3-4J^2(2\Delta+2\Delta_F-i\kappa)]A_2}, \\ C_{02g} &= \frac{16\sqrt{2}J^4E^2}{(2\Delta+2\Delta_F-i\kappa)[A_3-4J^2(2\Delta+2\Delta_F-i\kappa)]A_2},\end{aligned} \tag{16}$$

with

$$\begin{aligned}A_1 &= 2i\kappa(2\Delta+\Delta_F) - 4\Delta(\Delta+\Delta_F) + 4J^2 + \kappa^2, \\ A_2 &= 2i\kappa(2\Delta+\Delta_F) - 4\Delta(\Delta+\Delta_F) + 8J^2 + \kappa^2, \\ A_3 &= (2\Delta+\Delta_F-i\kappa)(2\Delta+2\Delta_F-i\kappa)^2, \\ A_4 &= 8J^4 - 4J^2(2\Delta-i\kappa)(2\Delta+2\Delta_F-i\kappa).\end{aligned} \tag{17}$$

According to the statistical properties of photons [9,55,56], the equal-time second-order correlation function is defined by

$$g_j^{(2)}(0) = \frac{\langle a_j^\dagger a_j^\dagger a_j a_j\rangle}{\langle a_j^\dagger a_j\rangle^2}, \tag{18}$$

which can be characterized the quantum statistics of nonclassical photons. Thus, the final analytical results are

$$\begin{aligned}g_1^{(2)}(0) &= \frac{2|C_{20g}|^2}{|C_{10g}|^4}, \\ g_2^{(2)}(0) &= \frac{2|C_{02g}|^2}{|C_{02g}|^4},\end{aligned} \tag{19}$$

which means the probability of simultaneous observation of two photons in the jth optical mode. The condition $g_j^{(2)}(0) < 1$ [$g_j^{(2)}(0) > 1$] stands for the photon blockade (photon-induced tunneling) effect.

C. Numerical simulation

To verify the analytical results and further demonstrate the quantum statistics of the photons, a numerical simulation method based on the quantum master equation is proposed. The system can be governed by the master equation

$$\dot{\rho} = -i[H'_{\mathrm{tot}}, \rho] + \kappa_1\mathcal{L}[a_1]\rho + \kappa_2\mathcal{L}[a_2]\rho + \gamma\mathcal{L}[\sigma_-]\rho, \tag{20}$$

where ρ is the dynamical density matrix of the system and $\mathcal{L}[o]\rho = o\rho o^\dagger - (o^\dagger o\rho + \rho o^\dagger o)/2$ denotes the standard Lindblad terms accounting for losses to the bath for an operator o ($o = a_1, a_2, \sigma_-$). To numerically examine the analysis, we focus on the statistical properties of the photons in

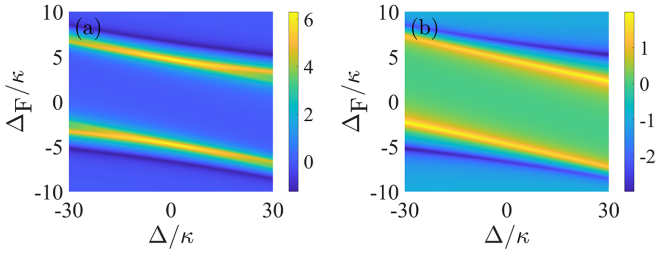

FIG. 2. The equal-time second-order correlation function (a) $g_1^{(2)}(0)$ and (b) $g_2^{(2)}(0)$ in logarithmic scale versus the optical detuning Δ and Fizeau shift Δ_F. The system parameters are $\kappa_1 = \kappa_2 = \gamma = \kappa$, $\Delta_c = \Delta_0 = \Delta$, $E/\kappa = 0.1$, and $J = 10\sqrt{2}\kappa$.

the corresponding optical modes, which can be described in terms of the normalized equal-time second-order correlation function [57]

$$g_j^{(2)}(0) = \frac{\langle a_j^{\dagger 2} a_j^2 \rangle}{\langle a_j^\dagger a_j \rangle^2} = \frac{\mathrm{Tr}(a_j^\dagger a_j^\dagger a_j a_j \rho_s)}{[\mathrm{Tr}(a_j^\dagger a_j \rho_s)]^2}, \tag{21}$$

where ρ_s is the steady-state solution after the long time evolution of the system. So far, the optimal Fizeau shifts Δ_{Fopt} are given by Eq. (13), as well as analytical and numerical results of second-order correlation functions representing the statistical properties of photons have been obtained. In the following, we numerically calculate the quantities of Eq. (21) and analyze the physical mechanism behind the emergence of nonreciprocal conventional photon blockades for the both optical modes.

IV. RESULTS AND DISCUSSION

In Figs. 2(a) and 2(b), we show the equal-time second-order correlation function $g_1^{(2)}(0)$ and $g_2^{(2)}(0)$ versus the frequency shift Δ_F and the detuning Δ on a logarithmic scale. The second-order correlation functions are derived by solving the master equation in Eq. (20) numerically. In the strong coupling regime $J = 10\sqrt{2}\kappa$, the photon antibunching phenomenon can be found simultaneously in both optical modes when the drive field ω_l is resonant with the one-photon resonant conditions, but is also off-resonant from the two-photon resonant conditions. The physical origin of the conventional photon blockade can be found based on the anharmonicity of the energy level spacing. Concretely, once the one-photon excitation is resonant, that is, $\Delta = \Delta_1^{(2)}$ or $\Delta = \Delta_1^{(3)}$, the subsequent transition (two-photon transition processes) is suppressed due to large detuning β_5 (please see Fig. 5 in detail), with

$$\beta_5 = \frac{1}{2}\left(\Delta_F - \sqrt{16J^2 + \Delta_F^2}\right) + \sqrt{8J^2 + \Delta_F^2}. \tag{22}$$

Under the strong coupling parameter regime, i.e., $J \gg \{\kappa_1, \kappa_2, \gamma\}$, a first excited photon with significant probability blocks the second one being excited due to large detuning β_5, which induces the single-photon blockade. In other words, an incident photon with the same frequency as the first excited $|\psi_1^{(3)}\rangle$ can excite the system from initial $|\psi_0\rangle$ to the first excited state $|\psi_1^{(3)}\rangle$, which means that only one photon can be detected in the system. Subsequently, the second photon with that frequency is emitted into the system. Due to the large detuning β_5, the second photon cannot be excited resonantly on the $|\psi_2^{(k)}\rangle$, which induces photon antibunching. According to Eq. (8), both optical modes a_1 and a_2 occupy the single-photon state, which indicates that single-photon antibunching can be simultaneously realized in both optical modes. The photon antibunching means that two optical modes tend to be occupied by one photon rather than multiple photons. In addition, we also find that, for a specific detuning Δ, when the sign of the Δ_F is different (driving devices in different directions), the phenomenon of photon bunching or photon antibunching occurs, which may observe nonreciprocal photon blockade under the appropriate parameter regime for the both optical modes.

In most cases, the nonreciprocal photon blockade effect is sensitive to cavity-mode driving, determining the resonance of the multiphoton physical transitions. For a precise observation of the nonreciprocal photon blockade, we present the dependence of the zero-delay-time second-order correlation functions $g_j^{(2)}(0)$ on optical detuning Δ when the Fizeau shift Δ_F takes different values through analytical and numerical methods, as shown in Fig 3.

In Figs. 3(a) and 3(b), the reciprocity conventional photon blockade phenomenon can be found due to the lack of Sagnac-Fizeau shift ($\Delta_F = 0$), where the locations of the two peaks $p_{n=4,5}$ correspond to the two-photon resonant excitation with the resonance conditions $\Delta = \Delta_2^{(4,5)}$. Moreover, the locations of the two dips $d_{n=2,3}$ correspond to single-photon resonant excitation $\Delta = \Delta_1^{(2,3)}$. It is not difficult to find that, in the curve of $g_j^{(2)}(0)$, the locations of these dips d_n and peaks p_n match the single-photon and two-photon resonance transition processes, respectively, which are consistent with our theoretical analysis performed in Sec. III A. More importantly, we can observe that the zero-delay-time second-order correlation function $g_j^{(2)}(0)$ exhibits strong nonreciprocity in both optical modes when the laser drives the optical mode a_1 from the different directions in Figs. 3(c) to 3(h). The two-photon resonance transition processes driven from the left side ($\Delta_F > 0$) are consistent with the driving frequency of the cavity field required by the single-photon resonance transition processes driven from the right side ($\Delta_F < 0$), that is, the nonreciprocal photon blockade effect occurs in the case of $\Delta = \Delta_1^{(2)} = \Delta_2^{(4)} \approx -17.76\kappa$ as shown in Figs. 3(c) and 3(e). One can set $\Delta = \Delta_1^{(3)} = \Delta_2^{(5)} \approx 17.76\kappa$ by changing the laser frequency ω_l, surprisingly, photon blockade to photon-induced tunneling conversion occurs in the same driving direction, ensuring the survival of the nonreciprocal photon blockade effect as shown in Figs. 3(d) and 3(f). Similar phenomena can be found in Figs. 3(g) and 3(h), in the case of $\Delta = \Delta_1^{(2)} = \Delta_2^{(4)} \approx -9.19\kappa$ or $\Delta = \Delta_1^{(3)} = \Delta_2^{(5)} \approx 9.19\kappa$. Moreover, we also find that there are four dips probably located at $\Delta \approx \pm 5.92\kappa$ and $\Delta \approx \pm 2.24\kappa$ as shown in Fig. 3(g), which originates from quantum interference between energy levels (please see Appendix A in detail).

To reveal the physical mechanism behind the nonreciprocal conventional photon blockade effect, the equal-time higher-order correlation function is introduced,

$$g_j^{(\mu)}(0) = \frac{\langle a_j^{\dagger\mu} a_j^\mu \rangle}{\langle a_j^\dagger a_j \rangle^\mu}, \tag{23}$$

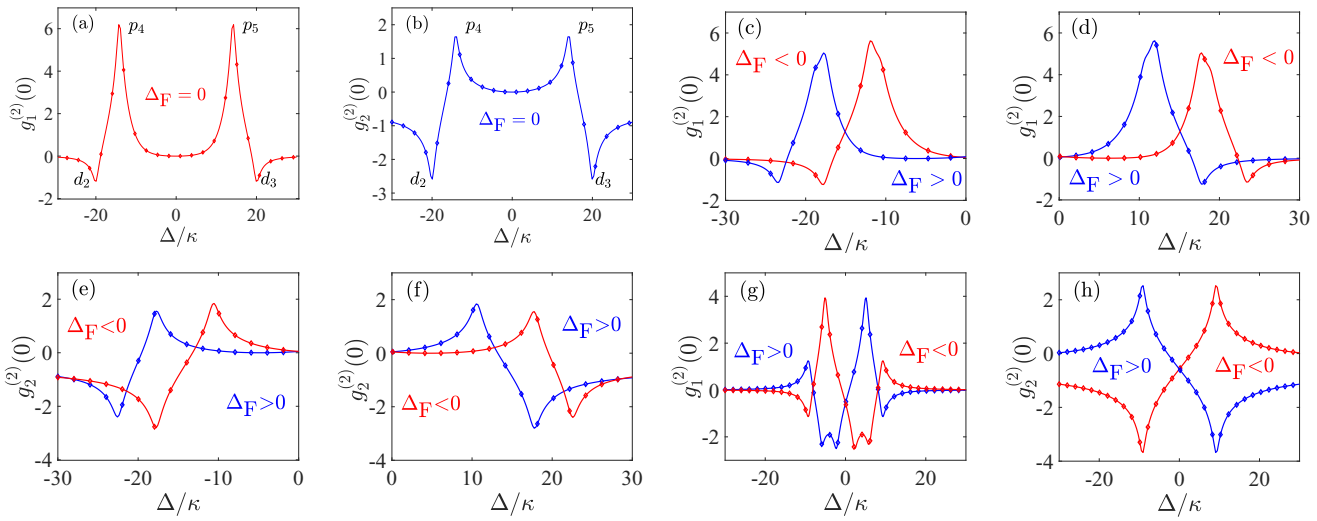

FIG. 3. The equal-time second-order correlation function $g_j^{(2)}(0)$ in logarithmic scale versus the optical detuning Δ with different Fizeau shift Δ_F. Analytical and numerical simulation results represented by red (blue) curve and red (blue) diamonds, respectively. Here $|\Delta_F| = \Delta_{\text{Fopt}}^{(1)}$ for (c)–(f), $|\Delta_F| = \Delta_{\text{Fopt}}^{(2)}$ for (g) and (h). In (a) and (b), $\Delta_F = 0$, which leads to the conventional reciprocal photon blockade caused by the anharmonicity of the system energy levels. In (c)–(h), $|\Delta_F| = \Delta_{\text{Fopt}}^{(1)}$ or $|\Delta_F| = \Delta_{\text{Fopt}}^{(2)}$, which leads to the nonreciprocal photon blockade. The other parameters are the same as in Fig. 2.

which can be used to explore the multiphoton blockade effect or multiphoton tunneling for specific values of μ ($\mu > 2$). For instance, $g_j^{(3)}(0) > 1$ ($g_j^{(3)}(0) < 1$) means that the third-order bunching (third-order antibunching) [34]. Moreover, it is well known that the two-photon blockade, that is, featuring three-photon antibunching but with two-photon bunching, which must meet the following terms [44]:

$$g_j^{(3)}(0) < f_j^{(3)} = e^{-\langle a_j^\dagger a_j\rangle},$$
$$g_j^{(2)}(0) > f_j^{(2)} = e^{-\langle a_j^\dagger a_j\rangle} + \langle a_j^\dagger a_j\rangle \times g_j^{(3)}(0). \quad (24)$$

To determine the type of nonreciprocal conventional photon blockade effect, we plot the time evolution of the corresponding optical correlation as shown in Fig. 4. In Figs. 4(a) and 4(b), we find that the statistics of photons in both optical modes exhibit an antibunching effect in the long-time limit, which implies the occurrence of the single-photon blockade and is consistent with the results in Figs. 3(c) and 3(e). Although the equal-time second-order correlation function shows a bunching effect, it violates the judgment criterion of the two-photon blockade given by Eq. (24), which means the photon-induced tunneling rather than the two-photon blockade effect occurs when the system is driven from the left side as shown in Figs. 4(c) and 4(d).

To better understand the physical origin behind the simultaneous nonreciprocal conventional photon blockades phenomenon, an energy-level diagram of the system is shown in Fig. 5 and the corresponding energy gaps can be calculated as (please see Appendix B in detail).

$$\beta_1 = \frac{1}{2}\left(\sqrt{8J^2 + \Delta_F^2} + \Delta_F\right),$$
$$\beta_2 = \frac{1}{2}\left(\sqrt{8J^2 + \Delta_F^2} - \Delta_F\right),$$
$$\beta_3 = \frac{1}{2}\left(\sqrt{16J^2 + \Delta_F^2} + \Delta_F\right),$$
$$\beta_4 = \frac{1}{2}\left(\sqrt{16J^2 + \Delta_F^2} - \Delta_F\right),$$
$$\beta_6 = \frac{1}{2}\sqrt{8J^2 + \Delta_F^2} - \frac{1}{4}\left(\sqrt{16J^2 + \Delta_F^2} - \Delta_F\right). \quad (25)$$

Specifically, with $\Delta = -17.76\kappa$ and driving from the right side ($\Delta_F < 0$), the driving field is in resonance with the single-photon transition $|\psi_0\rangle \to |\psi_1^{(3)}\rangle$ and the single-photon blockade occurs simultaneously for both optical modes. Physically, when the cavity field is driven from the right side by an externally driven laser with a frequency of ω_l, the

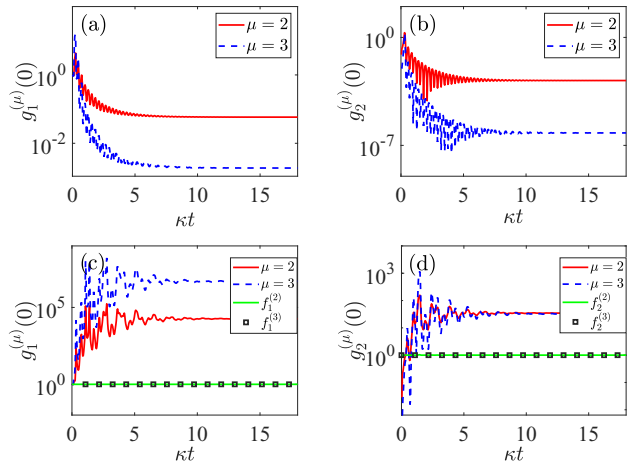

FIG. 4. The time evolution of the corresponding optical correlation with different Fizeau shift Δ_F. Here $\Delta = \Delta_1^{(2)} = \Delta_2^{(4)}$ and $\Delta_F = \Delta_{\text{Fopt}}^{(1)}$. In (a) and (b), the system is assumed to be driven from the right-hand side ($\Delta_F < 0$), while in (c) and (d), it is assumed to be driven from the left-hand side ($\Delta_F > 0$). The functions $f_j^{(2)}$ and $f_j^{(3)}$ are defined by Eq. (24), which is one of the criteria for multiphoton blockade. $\mu = 2$ or $\mu = 3$ denotes the order of the equal-time μ-order correlation function $g_1^{(\mu)}(0)$. The other parameters are the same as in Fig. 2.

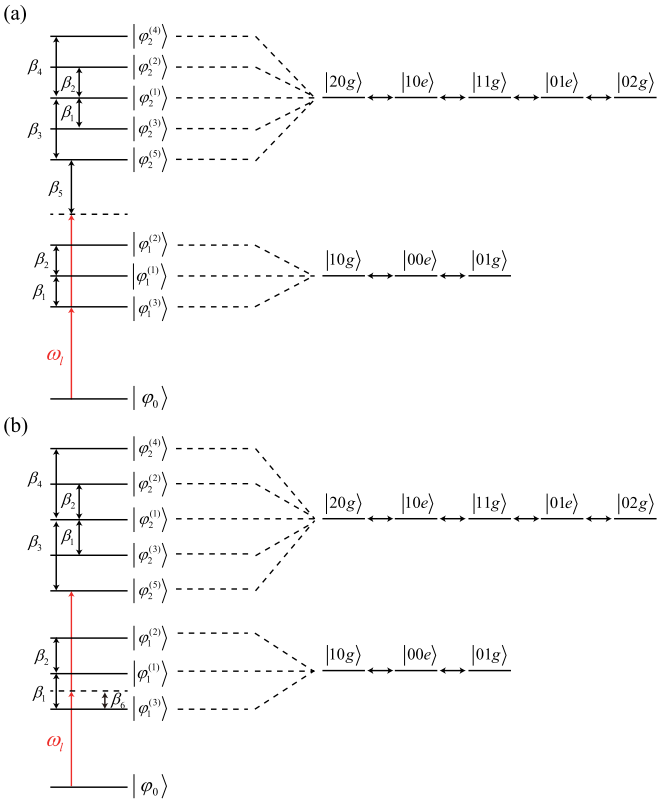

FIG. 5. Energy-level diagram of a simultaneously nonreciprocal conventional photon blockades in both independent optical modes. The eigenstates are drawn on the left-hand side. The photon conversion processes mediated by the two-level system between the two independent optical modes in one- and two-photon subspaces is plotted on the right-hand side. (a) Setting $\Delta = -17.76\kappa$, $J = 10\sqrt{2}\kappa$, and $\Delta_F \approx -4.76\kappa$, which means driving from the right side. (b) Setting $\Delta = -17.76\kappa, J = 10\sqrt{2}\kappa$, and $\Delta_F \approx 4.76\kappa$, which means driving from the left side.

photons with the same frequency will be excited and occupy the single-photon excited state $|\psi_1^{(3)}\rangle$, which enables the resonance transition from the vacuum state to the first excited state. Once the system has an first excited photon on $|\psi_1^{(3)}\rangle$ state, that photon will block the second one being excited due to the large detuning β_5 of the system. That is, there is not enough energy for the photon to be excited resonantly on the $|\psi_2^{(k)}\rangle$ state as shown in Fig. 5(a), so the photon antibunching effect occurs for both optical modes. On the other hand, when the cavity field is driven from the left side ($\Delta_F > 0$), the transition $|\psi_0\rangle \to |\psi_2^{(5)}\rangle$ is two-photon resonant, which means that two photons are resonantly excited and occupy the $|\psi_2^{(5)}\rangle$ state. Meanwhile, the single-photon transition $|\psi_0\rangle \to |\psi_1^{(k)}\rangle$ cannot be excited resonantly due to the large detuning β_6 as shown in Fig. 5(b), so the photon-induced tunneling can be observed. Similarly, the photon blockade to the photon-induced tunneling conversion occurs in different directions when $\Delta = 17.76\kappa$ or $\pm 9.19\kappa$. The essential reason is the change of energy level structure of the system under the different Fizeau-Sagnac shifts Δ_F.

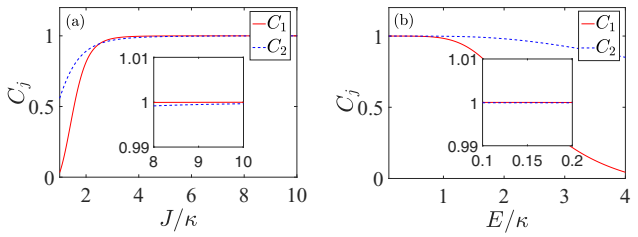

FIG. 6. (a) The bidirectional contrast ratio C_j versus the coupling strength J. (b) The bidirectional contrast ratio versus the amplitude of the external classical laser field E. For both (a) and (b), $\Delta_F = \Delta_{\text{Fopt}}^{(1)}$ and $\Delta = \Delta_1^{(2)}$. The other parameters are the same as in Fig. 2.

To quantitatively measure nonreciprocal photon blockade, the bidirectional contrast ratio C_j $(0 < C_j < 1)$ is introduced

$$C_j = \left| \frac{g_{jR}^{(2)}(0) - g_{jL}^{(2)}(0)}{g_{jR}^{(2)}(0) + g_{jL}^{(2)}(0)} \right|, \tag{26}$$

where the subscript R (L) represents the driving system from the right (left) side. Obviously, a larger C_j corresponds to a stronger nonreciprocal photon blockade effect. When $C_j = 1$, the perfect nonreciprocal photon blockade is achieved. From Fig. 6(a), it can be found that a larger coupling strength J corresponds to a stronger nonreciprocity. The reason is a stronger coupling strength J leads to a greater anharmonicity of the energy level spacing of the system, resulting in a photon antibunching. Similarly, we also find that a weak driving limit is necessary for strong nonreciprocity of the system as shown in Fig. 6(b). This is because the strong driving regime significantly increases the probability of photons in the excited state ($|20g\rangle$ and $|02g\rangle$), which destroys the photon antibunching. Photons in both optical modes have strong nonreciprocity when driving the device from different directions under the appropriate parameter regime ($C_j \approx 1$).

V. CONCLUSION

In conclusion, the simultaneously strong nonreciprocal photon blockades for both independent optical modes were studied in a rotating optical system, which was connected by a two-level system. The optimal Fizeau-Sagnac detunings can be obtained via the single-photon resonance and two-photon transition processes, which induce the nonreciprocal properties, that is, the simultaneous photon blockades occur when the spinning system is driven from an arbitrary direction but not from the other side under the appropriate parameters' regime. Moreover, the equal-time second-order correlation functions describing the photon blockades effect was obtained by solving the Schrödinger equation of the system analytically, which are in good agreement with numerical results by using quantum master equation. The physical mechanism behind the nonreciprocal conventional photon blockade is derived from the fact that Δ_F changes the energy level structure of the system. Meanwhile, the bidirectional contrast ratio C_j is also introduced to further explore the relationship between nonreciprocal strength and parameter fluctuations. Our scheme opens a prospective way to achieve simultaneous nonreciprocal photon blockades in both uncoupled optical

modes, which provides a promising method to generate the high-quality nonreciprocal single-photon source.

ACKNOWLEDGMENTS

This work was supported by the National Natural Science Foundation of China under Grants No. 12074330 and No. 12175033.

APPENDIX A: OPTIMAL DETUNING FROM THE UNCONVENTIONAL PHOTON BLOCKADE EFFECT

To make the photon distribution probability on the $|20g\rangle$ as low as possible, one can set $|C_{20g}| = 0$. Then the optimal detuning can be determined by the quartic equation

$$2\Delta^4 + k_3\Delta^3 + k_2\Delta^2 + k_1\Delta + k_0 = 0, \tag{A1}$$

where

$$\begin{aligned} k_0 &= J^4 + \frac{J^2\kappa^2}{2} - \Delta_F^2\kappa^2 + \frac{\kappa^4}{8}, \\ k_1 &= \Delta_F^3 - 2J^2\Delta_F - \frac{15}{4}\Delta_F\kappa^2, \\ k_2 &= 4\Delta_F^2 - 2J^2 - 3\kappa^2, \\ k_3 &= 5\Delta_F, \end{aligned} \tag{A2}$$

so the optimal conditions can be found

$$\begin{aligned} \Delta_{opt}^{(1,2)} &\approx -\frac{k_3}{8} - \frac{1}{2}\sqrt{\lambda_4} \pm \frac{1}{2}\sqrt{\lambda_5 - \frac{\lambda_6}{4\sqrt{\lambda_4}}}, \\ \Delta_{opt}^{(3,4)} &\approx -\frac{k_3}{8} + \frac{1}{2}\sqrt{\lambda_4} \pm \frac{1}{2}\sqrt{\lambda_5 + \frac{\lambda_6}{4\sqrt{\lambda_4}}}, \end{aligned} \tag{A3}$$

where

$$\begin{aligned} \lambda_1 &= k_2^2 - 3k_3k_1 + 24k_0, \\ \lambda_2 &= 2k_2^3 - 9k_3k_2k_1 + 54k_1^2 + 27k_3^2k_0 - 144k_2k_0, \\ \lambda_3 &= \frac{\sqrt[3]{2}\lambda_1}{6\sqrt[3]{\lambda_2 + \sqrt{-4\lambda_1^3 + \lambda_2^2}}} + \frac{\sqrt[3]{\lambda_2 + \sqrt{-4\lambda_1^3 + \lambda_2^2}}}{6\sqrt[3]{2}}, \\ \lambda_4 &= \frac{k_3^2}{16} - \frac{k_2}{3} + \lambda_3, \\ \lambda_5 &= \frac{k_3^2}{8} - \frac{2k_2}{3} - \lambda_3, \\ \lambda_6 &= -\frac{k_3^3}{8} + k_3k_2 - 4k_1. \end{aligned} \tag{A4}$$

For convenience, we redraw Fig. 3(g) in the main text and some special values of the optical detuning Δ are marked as shown in Fig. 7. Specifically, the two dips located at points a and c belong to the conventional photon blockade. However, the other four dips separately marked by the points e, f, g, and h originate from the unconventional photon blockade caused by different excitation pathways ($|10g\rangle \to |20g\rangle$ and $|10g\rangle \to |00e\rangle \to |10e\rangle \to |20g\rangle$), which can be obtained by Eq. (A3). Similar dips originating from the unconventional photon blockade cannot be found in Figs. 3(c) and 3(d) because Eq. (A1) is not satisfied in the real number space when $\Delta_F = \Delta_{Fopt}^{(1)}$. Here, we do not discuss them in detail.

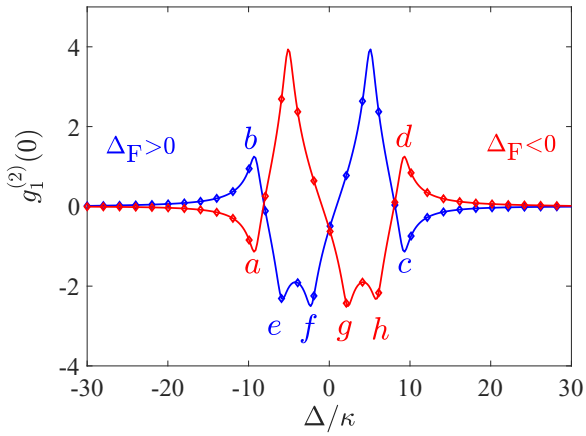

FIG. 7. The equal-time second-order correlation function $g_1^{(2)}(0)$ in logarithmic scale versus the optical detuning. Here $|\Delta_F| = \Delta_{Fopt}^{(1)}$. The other parameters are the same as in Fig. 2.

APPENDIX B: ENERGY GAPS OF THE SYSTEM EIGENSTATES

In this Appendix, we give the corresponding energy gaps of the system. According to Eq. (6), the eigenvalues of the system in the one-photon excitation subspace can be given by

$$\begin{aligned} E_1^{(1)} &= \omega_c + \Delta_F, \\ E_1^{(2,3)} &= \frac{1}{2}\left(\Delta_F \pm \sqrt{8J^2 + \Delta_F^2} + 2\omega_c\right). \end{aligned} \tag{B1}$$

Here $E_1^{(k)}$ denotes the eigenfrequency of the corresponding sublevel $|\psi_1^{(k)}\rangle$ in the one-photon excitation subspace. Therefore, the energy gaps in the one-photon excitation subspace can be calculated as

$$\begin{aligned} \beta_1 &= E_1^{(1)} - E_1^{(3)} \\ &= \frac{1}{2}\left(\sqrt{8J^2 + \Delta_F^2} + \Delta_F\right), \\ \beta_2 &= E_1^{(2)} - E_1^{(1)} \\ &= \frac{1}{2}\left(\sqrt{8J^2 + \Delta_F^2} - \Delta_F\right). \end{aligned} \tag{B2}$$

On the other hand, according to Eq. (10), the eigenvalues of the system in the two-photon excitation subspace are

$$\begin{aligned} E_2^{(1)} &= 2(\omega_c + \Delta_F), \\ E_2^{(2,3)} &= \frac{1}{2}\left(3\Delta_F \pm \sqrt{8J^2 + \Delta_F^2} + 4\omega_c\right), \\ E_2^{(4,5)} &= \frac{1}{2}\left(3\Delta_F \pm \sqrt{16J^2 + \Delta_F^2} + 4\omega_c\right). \end{aligned} \tag{B3}$$

Here $E_2^{(k)}$ denotes the eigenfrequency of the corresponding sublevel $|\psi_2^{(k)}\rangle$ in the two-photon excitation subspace.

Therefore, the energy gaps in the two-photon excitation subspace are

$$\begin{aligned}\beta_3 &= E_2^{(1)} - E_2^{(5)} \\ &= \frac{1}{2}\left(\sqrt{16J^2+\Delta_{\mathrm{F}}^2}+\Delta_{\mathrm{F}}\right), \\ \beta_4 &= E_2^{(4)} - E_2^{(1)} \\ &= \frac{1}{2}\left(\sqrt{16J^2+\Delta_{\mathrm{F}}^2}-\Delta_{\mathrm{F}}\right), \\ \beta_5 &= E_2^{(5)} - 2E_1^{(3)} \\ &= \frac{1}{2}\left(\Delta_{\mathrm{F}}-\sqrt{16J^2+\Delta_{\mathrm{F}}^2}\right)+\sqrt{8J^2+\Delta_{\mathrm{F}}^2}, \\ \beta_6 &= \frac{1}{2}E_2^{(5)} - E_1^{(3)} \\ &= \frac{1}{2}\sqrt{8J^2+\Delta_{\mathrm{F}}^2}-\frac{1}{4}\left(\sqrt{16J^2+\Delta_{\mathrm{F}}^2}-\Delta_{\mathrm{F}}\right). \end{aligned} \tag{B4}$$

[1] S. Ghosh and T. C. H. Liew, Single photons from a gain medium below threshold, Phys. Rev. B **97**, 241301 (2018).

[2] A. Alvarez-Fernandez, C. Cummins, M. Saba, U. Steiner, G. Fleury, V. Ponsinet, and S. Guldin, Block copolymer directed metamaterials and metasurfaces for novel optical devices, Adv. Opt. Mater. **9**, 2100175 (2021).

[3] F. Y. Hong and S. J. Xiong, Single-photon transistor using microtoroidal resonators, Phys. Rev. A **78**, 013812 (2008).

[4] H. Gorniaczyk, C. Tresp, J. Schmidt, H. Fedder, and S. Hofferberth, Single-Photon Transistor Mediated by Interstate Rydberg Interactions, Phys. Rev. Lett. **113**, 053601 (2014).

[5] N. Sangouard, C. Simon, H. de Riedmatten, and N. Gisin, Quantum repeaters based on atomic ensembles and linear optics, Rev. Mod. Phys. **83**, 33 (2011).

[6] D. Gerace, H. E. Türeci, A. Imamoglu, V. Giovannetti, and R. Fazio, The quantum-optical Josephson interferometer, Nat. Phys. **5**, 281 (2009).

[7] K. Y. Xia, F. Nori, and M. Xiao, Cavity-Free Optical Isolators and Circulators Using a Chiral Cross-Kerr Nonlinearity, Phys. Rev. Lett. **121**, 203602 (2018).

[8] K. M. Birnbaum, A. Boca, R. Miller, A. D. Boozer, T. E. Northup, and H. J. Kimble, Photon blockade in an optical cavity with one trapped atom, Nature (London) **436**, 87 (2005).

[9] P. Rabl, Photon Blockade Effect in Optomechanical Systems, Phys. Rev. Lett. **107**, 063601 (2011).

[10] X. Liang, Z. Duan, Q. Guo, S. Guan, M. Xie, and C. Liu, Photon blockade in a bimode nonlinear nanocavity embedded with a quantum dot, Phys. Rev. A **102**, 053713 (2020).

[11] W. Z. Zhang, J. Cheng, J. Y. Liu, and L. Zhou, Controlling photon transport in the single-photon weak-coupling regime of cavity optomechanics, Phys. Rev. A **91**, 063836 (2015).

[12] D. Pile, Single-photon transistor, Nat. Photon. **8**, 746 (2014).

[13] R. Trivedi, M. Radulaski, K. A. Fischer, S. H. Fan, and J. Vučković, Photon Blockade in Weakly Driven Cavity Quantum Electrodynamics Systems with Many Emitters, Phys. Rev. Lett. **122**, 243602 (2019).

[14] C. J. Zhu, Y. P. Yang, and G. S. Agarwal, Collective multiphoton blockade in cavity quantum electrodynamics, Phys. Rev. A **95**, 063842 (2017).

[15] D. Gerace and V. Savona, Unconventional photon blockade in doubly resonant microcavities with second-order nonlinearity, Phys. Rev. A **89**, 031803 (2014).

[16] S. L. Su, Y. Z. Tian, H. Z. Shen, H. P. Zang, E. J. Liang, and S. Zhang, Applications of the modified Rydberg antiblockade regime with simultaneous driving, Phys. Rev. A **96**, 042335 (2017).

[17] S. L. Su, Y. Gao, E. J. Liang, and S. Zhang, Fast Rydberg antiblockade regime and its applications in quantum logic gates, Phys. Rev. A **95**, 022319 (2017).

[18] D. Y. Wang, C. H. Bai, S. Liu, S. Zhang, and H. F. Wang, Distinguishing photon blockade in a $\mathcal{PT}$-symmetric optomechanical system, Phys. Rev. A **99**, 043818 (2019).

[19] D. Y. Wang, C. H. Bai, Y. Xing, S. Liu, S. Zhang, and H. F. Wang, Enhanced photon blockade via driving a trapped Λ-type atom in a hybrid optomechanical system, Phys. Rev. A **102**, 043705 (2020).

[20] A. Imamoğlu, H. Schmidt, G. Woods, and M. Deutsch, Strongly Interacting Photons in a Nonlinear Cavity, Phys. Rev. Lett. **79**, 1467 (1997).

[21] Y. H. Zhou, X. Y. Zhang, Q. C. Wu, B. L. Ye, Z. Q. Zhang, D. D. Zou, H. Z. Shen, and C. P. Yang, Conventional photon blockade with a three-wave mixing, Phys. Rev. A **102**, 033713 (2020).

[22] H. Y. Lin, X. Q. Wang, Z. H. Yao, and D. D. Zou, Kerr-nonlinearity enhanced conventional photon blockade in a second-order nonlinear system, Opt. Express **28**, 17643 (2020).

[23] X. W. Xu and Y. Li, Strong photon antibunching of symmetric and antisymmetric modes in weakly nonlinear photonic molecules, Phys. Rev. A **90**, 033809 (2014).

[24] X. W. Xu and Y. Li, Tunable photon statistics in weakly nonlinear photonic molecules, Phys. Rev. A **90**, 043822 (2014).

[25] H. Flayac and V. Savona, Unconventional photon blockade, Phys. Rev. A **96**, 053810 (2017).

[26] H. Jabri and H. Eleuch, Enhanced unconventional photon-blockade effect in one- and two-qubit cavities interacting with nonclassical light, Phys. Rev. A **106**, 023704 (2022).

[27] Z. G. Li, X. M. Li, and X. L. Zhong, Strong photon blockade in an all-fiber emitter-cavity quantum electrodynamics system, Phys. Rev. A **103**, 043724 (2021).

[28] A. Faraon, I. Fushman, D. Englund, N. Stoltz, P. Petroff, and J. Vučković, Coherent generation of non-classical light on a chip via photon-induced tunnelling and blockade, Nat. Phys. **4**, 859 (2008).

[29] K. Hou, C. J. Zhu, Y. P. Yang, and G. S. Agarwal, Interfering pathways for photon blockade in cavity QED with one and two qubits, Phys. Rev. A **100**, 063817 (2019).

[30] C. J. Zhu, K. Hou, Y. P. Yang, and L. Deng, Hybrid level anharmonicity and interference-induced photon blockade in a two-qubit cavity QED system with dipole-dipole interaction, Photon. Res. **9**, 1264 (2021).

[31] D. Y. Wang, C. H. Bai, S. T. Liu, S. Zhang, and H. F. Wang, Photon blockade in a double-cavity optomechanical system with nonreciprocal coupling, New J. Phys. **22**, 093006 (2020).

[32] H. Z. Shen, Y. H. Zhou, H. D. Liu, G. C. Wang, and X. X. Yi, Exact optimal control of photon blockade with weakly nonlinear coupled cavities, Opt. Express **23**, 32835 (2015).
[33] I. Carusotto and C. Ciuti, Quantum fluids of light, Rev. Mod. Phys. **85**, 299 (2013).
[34] K. Wang, Q. Wu, Y. F. Yu, and Z. M. Zhang, Nonreciprocal photon blockade in a two-mode cavity with a second-order nonlinearity, Phys. Rev. A **100**, 053832 (2019).
[35] R. J. Potton, Reciprocity in optics, Rep. Prog. Phys. **67**, 717 (2004).
[36] M. Mansuripur, Reciprocity in classical linear optics, Opt. Photonics News **9**, 53 (1998).
[37] L. Feng, M. Ayache, J. Q. Huang, Y. L. Xu, M. H. Lu, Y. F. Chen, Y. Fainman, and A. Scherer, Nonreciprocal light propagation in a silicon photonic circuit, Science **333**, 729 (2011).
[38] A. Parra-Rodriguez, I. L. Egusquiza, D. P. DiVincenzo, and E. Solano, Canonical circuit quantization with linear nonreciprocal devices, Phys. Rev. B **99**, 014514 (2019).
[39] C. Leroux, A. Parra-Rodriguez, R. Shillito, A. D. Paolo, W. D. Oliver, C. M. Marcus, M. Kjaergaard, A. Gyenis, and A. Blais, Nonreciprocal devices based on voltage-tunable junctions, arXiv:2209.06194.
[40] D. L. Sounas and A. Alù, Non-reciprocal photonics based on time modulation, Nat. Photon. **11**, 774 (2017).
[41] Y. Shoji and T. Mizumoto, Magneto-optical non-reciprocal devices in silicon photonics, Sci. Technol. Adv. Mater. **15**, 014602 (2014).
[42] X. Y. Xu, G. H. Ren, T. Feleppa, X. M. Liu, A. Boes, A. Mitchell, and A. J. Lowery, Self-calibrating programmable photonic integrated circuits, Nat. Photon. **16**, 595 (2022).
[43] Y. L. Ren, S. L. Ma, J. K. Xie, X. K. Li, M. T. Cao, and F. L. Li, Nonreciprocal single-photon quantum router, Phys. Rev. A **105**, 013711 (2022).
[44] R. Huang, A. Miranowicz, J. Q. Liao, F. Nori, and H. Jing, Nonreciprocal Photon Blockade, Phys. Rev. Lett. **121**, 153601 (2018).
[45] B. Li, R. Huang, X. Xu, A. Miranowicz, and H. Jing, Nonreciprocal unconventional photon blockade in a spinning optomechanical system, Photon. Res. **7**, 630 (2019).
[46] J. Wang, Q. Wang, and H. Z. Shen, Nonreciprocal unconventional photon blockade with spinning atom-cavity, Europhys. Lett. **134**, 64003 (2021).
[47] X. Shang, H. Xie, and X. M. Lin, Nonreciprocal photon blockade in a spinning optomechanical resonator, Laser Phys. Lett. **18**, 115202 (2021).
[48] W. S. Xue, H. Z. Shen, and X. X. Yi, Nonreciprocal conventional photon blockade in driven dissipative atom-cavity, Opt. Lett. **45**, 4424 (2020).
[49] S. Maayani, R. Dahan, Y. Kligerman, E. Moses, A. U. Hassan, H. Jing, F. Nori, D. N. Christodoulides, and T. Carmon, Flying couplers above spinning resonators generate irreversible refraction, Nature (London) **558**, 569 (2018).
[50] Y. T. Guo, F. Zou, J. F. Huang, and J. Q. Liao, Retrieval of photon blockade effect in the dispersive Jaynes-Cummings model, Phys. Rev. A **105**, 013705 (2022).
[51] Y. W. Jing, H. Q. Shi, and X. W. Xu, Nonreciprocal photon blockade and directional amplification in a spinning resonator coupled to a two-level atom, Phys. Rev. A **104**, 033707 (2021).
[52] J. K. Xie, S. L. Ma, and F. L. Li, Quantum-interference-enhanced magnon blockade in an yttrium-iron-garnet sphere coupled to superconducting circuits, Phys. Rev. A **101**, 042331 (2020).
[53] M. B. Plenio and P. L. Knight, The quantum-jump approach to dissipative dynamics in quantum optics, Rev. Mod. Phys. **70**, 101 (1998).
[54] H. Z. Shen, Q. Wang, J. Wang, and X. X. Yi, Nonreciprocal unconventional photon blockade in a driven dissipative cavity with parametric amplification, Phys. Rev. A **101**, 013826 (2020).
[55] Y. Liu, A. Miranowicz, Y. B. Gao, J. Bajer, C. P. Sun, and F. Nori, Qubit-induced phonon blockade as a signature of quantum behavior in nanomechanical resonators, Phys. Rev. A **82**, 032101 (2010).
[56] M. Li, Y. L. Zhang, S. H. Wu, C. H. Dong, X. B. Zou, G. C. Guo, and C. L. Zou, Single-Mode Photon Blockade Enhanced by Bi-Tone Drive, Phys. Rev. Lett. **129**, 043601 (2022).
[57] K. Mølmer, Y. Castin, and J. Dalibard, Monte Carlo wavefunction method in quantum optics, J. Opt. Soc. Am. B **10**, 524 (1993).